

Emergent fermionic gauge theory and foliated fracton order in the Chamon modelWilbur Shirley,^{1,2} Xu Liu,^{3,*} and Arpit Dua^{1,2}¹*School of Natural Sciences, Institute for Advanced Study, Princeton, New Jersey 08540, USA*²*Department of Physics and Institute for Quantum Information and Matter,
California Institute of Technology, Pasadena, California 91125, USA*³*Mani L. Bhaumik Institute for Theoretical Physics, Department of Physics and Astronomy,
University of California at Los Angeles, Los Angeles, California 90095, USA*

(Received 1 July 2022; accepted 28 October 2022; published 20 January 2023)

The Chamon model is an exactly solvable spin Hamiltonian exhibiting nontrivial fracton order. In this paper, we dissect two distinct aspects of the model. First, we show that it exhibits an emergent fractonic gauge theory coupled to a fermionic subsystem symmetry-protected topological state under four stacks of \mathbb{Z}_2 planar symmetries. Second, we show that the Chamon model hosts 4-foliated fracton order by describing an entanglement renormalization group transformation that exfoliates four separate stacks of 2D toric codes from the bulk system.

DOI: [10.1103/PhysRevB.107.035136](https://doi.org/10.1103/PhysRevB.107.035136)**I. INTRODUCTION**

Gapped quantum systems can form nontrivial phases of matter in the absence of symmetry if they exhibit long-range entanglement in the many-body ground state [1]. The traditional examples of long-range entangled phases are those with intrinsic topological order such as fractional quantum Hall states [2,3] and discrete gauge theories [4,5], which are characterized at low energy by topological quantum field theories [6]. In 2005, Chamon discovered a three-dimensional exactly solvable lattice model [7] that represents the first example of a unique kind of long-range entangled order known as *fractonic order* [8,9].

Quantum phases with fractonic order cannot be described by topological quantum field theory due to an intertwining of universal properties with lattice geometry [8–11]. In particular, fractonic orders are characterized by a ground state degeneracy (GSD) that scales exponentially with linear system size and the existence of fractional excitations with constrained mobility [9,12–15]. The Chamon model, for instance, harbors three kinds of quasiparticles: *planons*, which are mobile within a plane; *lineons*, which can move along a line; and *fractons*, which are fundamentally immobile as individual particles [12]. In recent years, a wide range of fracton orders have been discovered theoretically, each exhibiting a different manifestation of constrained quasiparticle mobility and subextensive GSD [8,9,11,13–48]. Notable examples include the Haah cubic code [13] and the X-cube model [9]. It is natural to ask how the variety of fractonic orders can be systematically characterized within a common theoretical framework.

Many fractonic orders have a unified characterization as emergent gauge theories of discrete *subsystem* symmetries, which have either planar or fractal geometry [9,49–51]. For example, the X-cube model is obtained by gauging three orthogonal sets of planar Ising symmetries of a cubic lattice spin-1/2 paramagnet (referred to as a *3-foliated* gauge theory) [9]. The gauging procedure has been extended to fermion parity subsystem symmetries in fermionic systems, whose gauging yields gapped fractonic gauge theories with emergent fermionic charges [52,53]. On one hand, a large class of fractonic orders, including those belonging to the class of Calderbank-Shor-Steane (CSS) stabilizer codes, can be obtained via this procedure [51]. On the other hand, it remains unclear how, or if, certain fracton models, including the Chamon model, can be obtained by gauging and hence characterized by emergent gauge theory.

In a parallel development, the concept of *foliated fracton order* (FFO) was recently introduced in an effort to systematically characterize fractonic orders with planon excitations [50,54]. A lattice model is said to have FFO if the lattice size can be systematically reduced by removing, or *exfoliating*, layers of 2D topological orders from the bulk 3D system via a finite-depth quantum circuit. Such a transformation maps a subset of the bulk planon excitations into anyons of the exfoliated 2D orders. For instance, for the X-cube model, it is possible to exfoliate layers of 2D toric code normal to the three cubic lattice directions, hence the X-cube model is said to have a *3-foliation* structure. The notion of FFO has been shown to apply to a large class of models beyond the X-cube model [55–57]. However, thus far it has remained unknown whether the fractonic order of the Chamon model is foliated.

The purpose of this paper is to fill the gaps in the fracton literature by presenting two results on the Chamon model. First, we show that the model is characterized by a 4-foliated gauge theory coupled to a fermionic subsystem symmetry-protected topological (SSPT) state. In other words, it can be obtained

*Current address: Facebook Inc., Menlo Park, California 94025, USA.

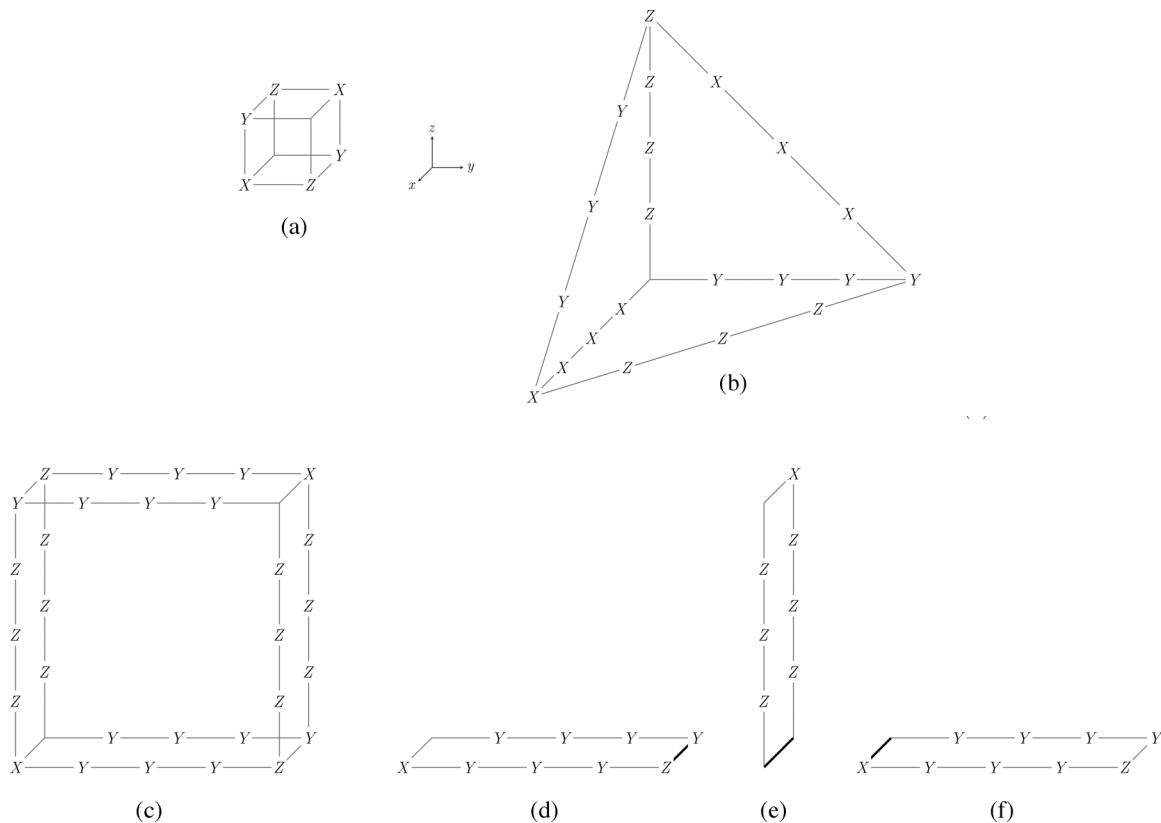


FIG. 1. (a) The operator O_c , which is a tensor product of the six Pauli operators. (b) A tetrahedral wire-frame operator, which is equal to a product of O_c operators inside the tetrahedron. (c) A loop operator for an elementary planon of the Chamon model, which is a product of O_c operators within the loop. (d)–(f) Three planon string operators W_3 , W_2 , and W_1 forming a T junction (the bold edge represents the same edge in each subfigure). The fermionic exchange statistic of the elementary planon is given by $W_3 W_2^\dagger W_1 W_3^\dagger W_2 W_1^\dagger = -1$

by gauging four sets of planar \mathbb{Z}_2 symmetries that protect a nontrivial SSPT state [38,58] in a fermionic lattice system and then performing a local unitary transformation. This is a surprising result because there is no *a priori* clear division of fractional excitations into gauge charge and gauge flux sectors (as is the case for CSS codes). Instead, it is necessary to expand the unit cell and divide the excitations into charge and flux sectors according to the sublattice on which they reside. This is reminiscent of the gauge theory description of the much simpler 2D Wen plaquette model [59].

Second, we show that the Chamon model exhibits FFO with a 4-foliation structure composed of 2D toric code resource layers. In particular, we describe an entanglement renormalization (ER) group transformation [22,60,61] that maps a copy of the Chamon model on a $3L \times 3L \times 3L$ cubic lattice to a coarse-grained Chamon model on an $L \times L \times L$ lattice tensored with four decoupled stacks of 2D toric codes. This 4-foliation structure is consistent with the four orientations of planons in the Chamon model, and is most easily described in terms of the action of the transformation on the planon excitations. We have also obtained an explicit translation-invariant Clifford circuit realizing this transformation.

The paper is organized as follows. In Sec. II, we review the Chamon model and its essential properties. In Sec. III, we explain the characterization of the Chamon model in terms of emergent fermionic gauge theory. In Sec. IV, we describe

the FFO exhibited by the Chamon model. We conclude with a discussion in Sec. V.

II. THE CHAMON MODEL

The Chamon model was originally defined on an FCC lattice with one qubit per site [7,12], exhibiting the tetrahedral point group symmetry of the lattice. For our purposes, it will be more convenient to place the model on a cubic lattice with one qubit per site by performing an isometry of \mathbb{R}_3 defined by

$$\begin{aligned} (0, \frac{1}{2}, \frac{1}{2}) &\rightarrow (1, 0, 0), \\ (\frac{1}{2}, 0, \frac{1}{2}) &\rightarrow (0, 1, 0), \\ (\frac{1}{2}, \frac{1}{2}, 0) &\rightarrow (0, 0, 1). \end{aligned} \quad (1)$$

In this formulation, the Hamiltonian has the form

$$H_C = - \sum_c O_c, \quad (2)$$

where c indexes the elementary cubes of the lattices and O_c is the six-body Pauli operator depicted in Fig. 1(a). For any pair of cubes c, c' , it holds that $[O_c, O_{c'}] = 0$, thus H_C is an exactly solvable stabilizer code Hamiltonian [62]. The GSD of the model on an $L_x \times L_y \times L_z$ periodic cubic lattice has the form

$$\log_2 \text{GSD} = L_x + L_y + L_z + \gcd(L_x, L_y, L_z) - 3, \quad (3)$$

The linear component of this formula arises from the following relations between stabilizer generators:

$$\prod_{c \in P} O_c = 1, \quad (4)$$

where P is any dual lattice plane normal to the x , y , z , or $w = (1, 1, 1)$ directions. This gives a total of $L_x + L_y + L_z + L_w$ relations, where $L_w = \gcd(L_x, L_y, L_z)$ is the number of planes normal to w under periodic boundary conditions. However, not all of these relations are independent. The global relation between all Hamiltonian terms is generated by the product of all planar relations for each of the four directions. Hence, there are three redundant relations leading to the constant correction in Eq. (4).

The model hosts fractional excitations of all mobility types: fractons, lineons, and planons. This structure can be understood by examining the quasiparticle creation operators. First, lineons are created at the endpoints of truncated segments of rigid wire-frame operators, which are products of all O_c terms within a given polyhedral region bounded by x , y , z , and w planes. Due to the relations in Eq. (4), such an operator is supported on the edges of the polyhedron, for instance, the tetrahedral wire-frame operator pictured in Fig. 1(b). There are six kinds of lineons, with mobility in the x , y , z , $(0, 1, -1)$, $(-1, 0, 1)$, and $(1, -1, 0)$ directions, respectively. They obey triple fusion rules in which three distinctly oriented lineons fuse together into the vacuum, which is possible when their respective string operators form the corner of a wire-frame operator. For example, both the x , y , z lineon triple and the $(1, -1, 0)$, $(0, 1, -1)$, z lineon triple fuse into the vacuum, whereas x , y , $(1, -1, 0)$ and x , y , $(-1, 0, 1)$ triples do not. A lineon corresponds to an excitation of a pair of (next-nearest neighbor) Hamiltonian terms.

Fractons, on the other hand, correspond to excitations of a single isolated Hamiltonian term and are created at the corners of membrane operators. For instance, consider the action of a single Pauli Z operator at the origin. This excites four Hamiltonian terms centered around $(1/2, -1/2, -1/2)$, $(1/2, -1/2, 1/2)$, $(-1/2, 1/2, -1/2)$, and $(-1/2, 1/2, 1/2)$. Hence, a large rectangular membrane of Pauli Z operators within a plane normal to the $(1,1,0)$ direction will excite four isolated Hamiltonian terms at the corners of the membrane. There are equivalent membrane operators normal to the $(0,1,1)$ and $(1,0,1)$ directions composed of Pauli X and Y operators, respectively.

Finally, there are four types of planons mobile within planes normal to the x , y , z , and w directions, respectively. For each direction, there is one independent species of planon per lattice spacing, referred to as an elementary planon. A closed string operator for an elementary planon can be obtained by taking the product of all O_c operators in a large region within a single x , y , z , or w plane, for instance, as depicted in Fig. 1(c). There are two important features: First, each of the elementary planons has fermionic exchange statistics. Second, adjacent parallel planons have a mutual π braiding statistic. These facts can be verified by examining the structure of the planon string operators as shown in Figs. 1(d)–1(f). Since the elementary planons can be regarded as lineon dipoles, this also implies that intersecting lineons have a mutual π braiding statistic.

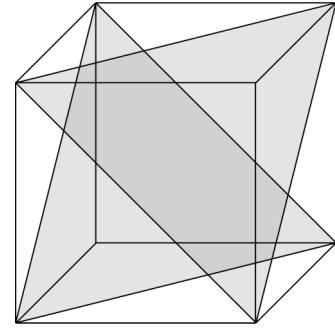


FIG. 2. The tetrahedral-octahedral honeycomb. Each cube of a cubic lattice is split into two tetrahedra and one octahedron by $(1,1,1)$ planes (shaded).

III. EMERGENT FERMIONIC GAUGE THEORY

In this section, we demonstrate that the Chamon model is equivalent under a generalized local unitary (gLU) transformation [1] to a fractonic gauge theory coupled to a fermionic SSPT state [38,58]. We begin with the SSPT matter Hamiltonian H_M , which is symmetric under four stacks of \mathbb{Z}_2 planar symmetries. We then gauge the symmetry to obtain a spin model H_G . Finally, we transform H_G into the Chamon model H_C via a gLU.

We also sketch an argument that H_M is a weak SSPT in the sense of Refs. [63,64].

A. Matter Hamiltonian

First, we describe the matter Hamiltonian H_M . We consider a cellulation of \mathbb{R}_3 obtained by slicing along lattice planes of integer spacing normal to the x , y , z , and $w = (1, 1, 1)$ directions. The x , y , and z planes divide \mathbb{R}_3 into unit volume elementary cubes, and each cube is further sliced into three 3-cells by the w planes: two types of tetrahedra and one octahedron, as pictured in Fig. 2. The Hilbert space of H_M is composed of one fermionic orbital per tetrahedron and one qubit per octahedron. The Hamiltonian has the form

$$H_M = - \sum_t i\gamma_t \gamma'_t - \sum_o \mathcal{X}_o, \quad (5)$$

where γ_t indicates the fermion at tetrahedra t , \mathcal{X}_o indicates the Pauli X operator that acts on the qubit of the octahedra o , and

$$\mathcal{X}_o \equiv X_o \prod_{a=0}^1 \prod_{b=0}^1 \prod_{c=0}^1 \prod_{d=0}^1 Z_{o+a\hat{x}-b\hat{y}+c(1,-1,0)+d(-1,0,1)}, \quad (6)$$

where $o + \vec{r}$ represents the octahedron displaced from o by \vec{r} [see Fig. 3(a)]. The terms of H_M mutually commute, hence the model is exactly solvable.

H_M is symmetric under four stacks of unitary \mathbb{Z}_2 planar subsystem symmetries, normal to the x , y , z , and w directions. Each symmetry generator is associated with a dual lattice plane of the tetrahedral-octahedral honeycomb. Let P denote the set of all 3-cells lying in a dual lattice plane. Then the corresponding symmetry of H_M is

$$S_P = \prod_{t \in P} i\gamma_t \gamma'_t \prod_{o \in P} X_o. \quad (7)$$

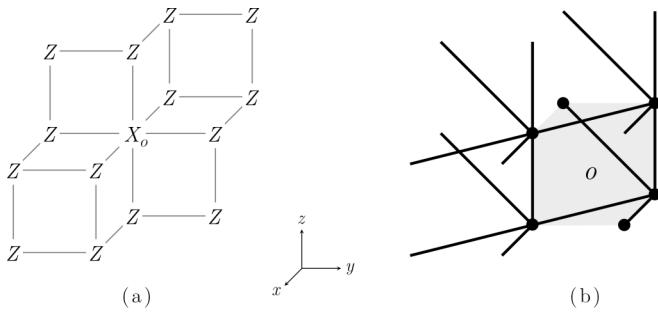


FIG. 3. (a) Depiction of the operator \mathcal{X}_o . Each Pauli operator acts on an octahedral qubit, whose center points form a cubic lattice. The octahedron o is indicated by subscript. (b) The set of edges E_o with respect to the octahedron o , whose vertices are the six dots.

There is one symmetry generator for every such P . To see that the \mathcal{X}_o terms commute with all of these symmetries, note that each of the x , y , z , and w planes contains at least one of the \hat{y} , \hat{z} , $(1, -1, 0)$, or $(-1, 0, 1)$ vectors.

We note that the subsystem symmetries obey the global relations

$$\prod_{P_x} S_{P_x} = \prod_{P_y} S_{P_y} = \prod_{P_z} S_{P_z} = \prod_{P_w} S_{P_w}, \quad (8)$$

where the products are over all dual lattice planes P_μ normal to μ . Importantly, we also note that the product of symmetries over all *even* dual lattice planes in all four directions is equal to the *global* fermion parity \mathbb{Z}_2^F , which is thus generated by the subsystem symmetry group. Therefore, a bosonic system will be obtained upon gauging the symmetries.

B. Gauging

We now discuss the gauging of symmetries according to the general prescription [50,52,53,65]. The first step is to identify a set of minimal couplings that generate the algebra of symmetric operators together with the on-site symmetry representations (Pauli X on qubits and $i\gamma\gamma'$ on fermion orbitals). There is one minimal coupling for each edge e of the tetrahedral-octahedral honeycomb, acting on the degrees of freedom associated with the four 3-cells adjacent to e (two octahedra o and o' and two oppositely oriented tetrahedra t and t'), which we choose to be

$$M_e \equiv Z_o Z_{o'} \gamma_t \gamma_{t'}. \quad (9)$$

The second step is to introduce a gauge qubit degree of freedom for each minimal coupling, hence one per edge. We simultaneously restrict the Hilbert space by introducing generalized Gauss's law constraints for each matter degree of freedom. The constraints have the form

$$X_o \prod_{e \in o} X_e = 1, \quad i\gamma_t \gamma_{t'} \prod_{e \in t} X_e = 1 \quad (10)$$

for each octahedron o and tetrahedron t .

The third step is to couple the gauge and matter degrees of freedom by introducing a gauged Hamiltonian that preserves the constraints. In particular, in the gauged Hamiltonian, the minimal coupling for each edge e is composed with the gauge

qubit operator Z_e :

$$M_e \rightarrow M_e Z_e. \quad (11)$$

This modification is nonunique, since there are multiple ways to express the operator \mathcal{X}_o in terms of the minimal couplings. We choose the expression

$$\mathcal{X}_o = X_o \prod_{e \in E_o} M_e, \quad (12)$$

where E_o is the set of edges depicted in Fig. 3(b). Hence,

$$\mathcal{X}_o \rightarrow X_o \prod_{e \in E_o} M_e Z_e. \quad (13)$$

The final step is to add a set of terms $B_{v,\mu}$ for each vertex v to the gauged Hamiltonian to gap out the gauge flux excitations. Here $\mu = x, y, z, w$ and $B_{v,\mu}$ is defined as the tensor product of Pauli Z operators over the six links adjacent to v in the plane normal to μ . Thus, the gauged Hamiltonian takes the form

$$\tilde{H}_M = - \sum_t i\gamma_t \gamma_{t'} - \sum_o X_o \prod_{e \in E_o} M_e Z_e - \sum_{v,\mu} B_{v,\mu}, \quad (14)$$

subject to the constraints Eqs. (10).

The matter degrees of freedom can be eliminated via the unitary

$$\begin{aligned} X_o &\rightarrow X_o \prod_{e \in o} X_e, & Z_o &\rightarrow Z_o, \\ \gamma_t &\rightarrow \gamma_t \prod_{e \in t} X_e, & \gamma_{t'} &\rightarrow \gamma_{t'}, \\ X_e &\rightarrow X_e, & Z_e &\rightarrow M_e \bar{Z}_e, \end{aligned} \quad (15)$$

which maps the constraints of Eqs. (10) to $X_o = 1$ and $i\gamma_t \gamma_{t'} = 1$, respectively. The \bar{Z}_e operators are defined in Fig. 4 such that \bar{Z}_e and $\bar{Z}_{e'}$ anticommute if e and e' belong to the same tetrahedron, and commute otherwise. In the constrained space, \tilde{H}_M is mapped to a bosonic Hamiltonian H_G acting on the pure gauge qubit Hilbert space:

$$H_G = - \sum_t \bar{A}_t - \sum_o \bar{A}_o - \sum_{v,\mu} \bar{B}_{v,\mu}, \quad (16)$$

where

$$\bar{A}_t \equiv \prod_{e \in t} X_e, \quad \bar{A}_o \equiv \prod_{e \in o} X_e \prod_{e \in E_o} \bar{Z}_e, \quad (17)$$

and $\bar{B}_{v,\mu}$ is the image of $B_{v,\mu}$ under the unitary Eqs. (15). The terms of H_G mutually commute, hence they define a Pauli stabilizer code.

C. Excitation content and ground-state degeneracy of the gauged Hamiltonian

To analyze the properties of H_G , it is helpful to express the Hamiltonian in terms of operators \bar{X}_e and \bar{Z}_e associated with edge e of the tetrahedral-octahedral honeycomb. These operators are defined in Fig. 4. We have already used the \bar{Z}_e operators in the unitary Eqs. (15). In particular,

$$\bar{A}_c = \prod_{e \in c} \bar{X}_e, \quad \bar{B}_{v,\mu} = \prod_{v \ni e \perp \mu} \bar{Z}_e, \quad (18)$$

where the second product is over the six edges e adjacent to v in the plane normal to μ . These operators are defined in Fig. 4

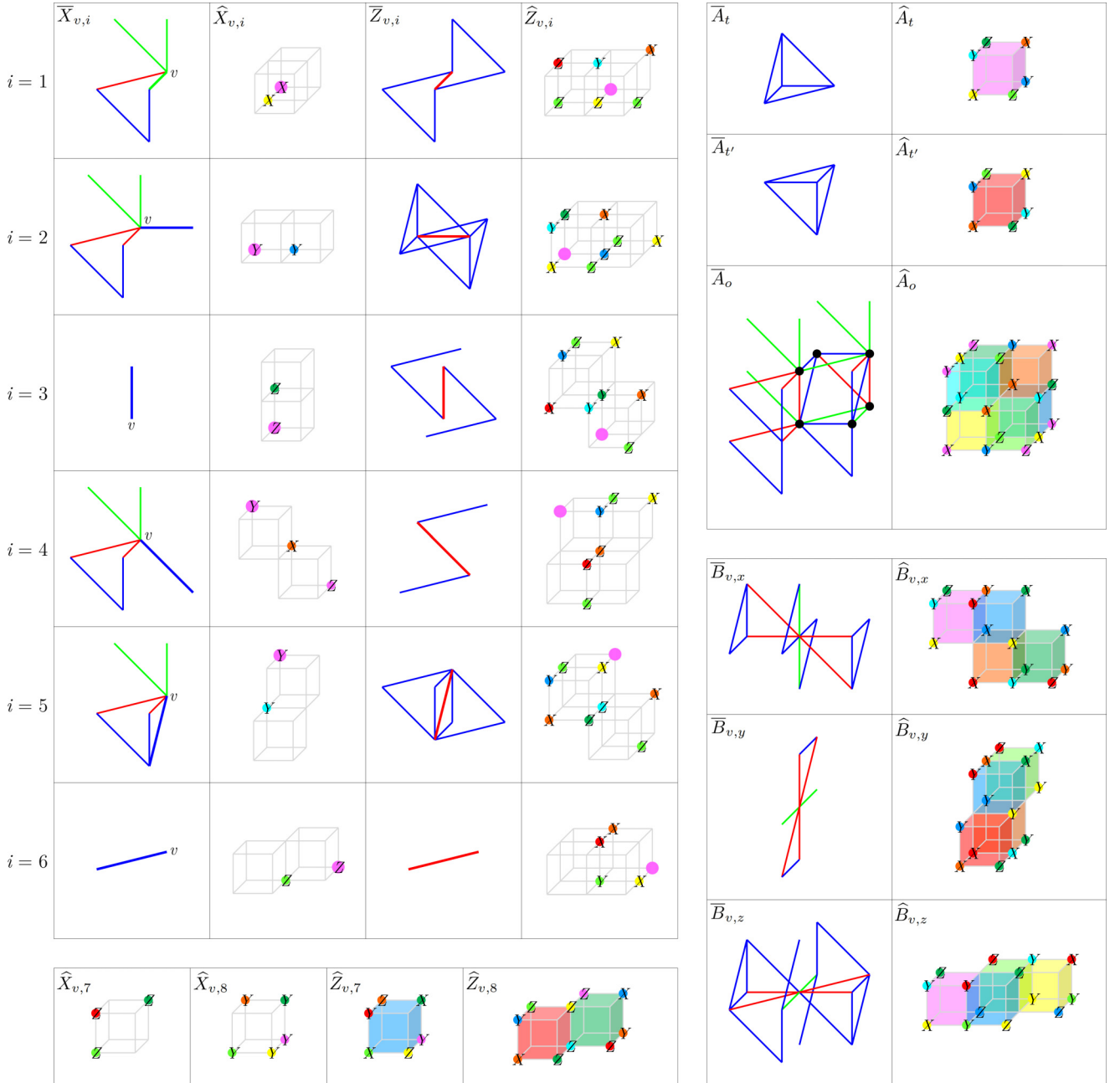


FIG. 4. Definitions of the Pauli operators introduced in this section. The operators $\bar{X}_{v,i}$ and $\bar{Z}_{v,i}$ acting on \mathcal{H}_G for $i = 1, \dots, 6$ are defined in the table on the left, which are equivalent to the \bar{X}_e and \bar{Z}_e operators for the bold edge e . Red, green, and blue edges, respectively, represent the action of Pauli Z , Y , and X . The operators $\hat{X}_{v,i}$ and $\hat{Z}_{v,i}$ acting on \mathcal{H}_C for $i = 1, \dots, 8$ are defined in the tables on the left, with v given by the enlarged magenta dot in each figure (an unlabeled enlarged dot has no Pauli action). The 3-cell operators \bar{A}_t , $\bar{A}_{t'}$, and \bar{A}_o , and vertex operators $\bar{B}_{v,\mu}$ of \mathcal{H}_G are defined in the tables on the right. The vertices of octahedron o are indicated by black dots, whereas the vertex v for each $\bar{B}_{v,\mu}$ operator is the central vertex. The operators \hat{A}_t , $\hat{A}_{t'}$, \hat{A}_o , $\hat{B}_{v,x}$, $\hat{B}_{v,y}$, and $\hat{B}_{v,z}$ acting on \mathcal{H}_C are likewise defined in the tables on the right. These operators, together with $\hat{Z}_{v,7}$ and $\hat{Z}_{v,8}$, generate the stabilizer group of \mathcal{H}_C . The shaded cubes indicate that a given operator is equal to a product of the corresponding cube terms of \mathcal{H}_C (the color of each cube corresponds to the vertex of minimum x , y , and z coordinates).

and satisfy the relations

$$\bar{X}_e^2 = \bar{Z}_e^2 = 1, \quad \{\bar{X}_e, \bar{Z}_e\} = [\bar{X}_e, \bar{Z}_{e'}] = 0, \quad (19)$$

where e and e' are distinct edges. On the other hand, if e and e' are nearby, then it is generically the case that

$$[\bar{X}_e, \bar{X}_{e'}] \neq 0, \quad [\bar{Z}_e, \bar{Z}_{e'}] \neq 0. \quad (20)$$

It is instructive to note that due to Eqs. (18), there is a formal relation between \mathcal{H}_G and a certain 4-foliated version of the X-cube model, \mathcal{H}_{4XC} , described in Appendix A. Roughly speaking, \mathcal{H}_G is obtained from \mathcal{H}_{4XC} by replacing $X_e \rightarrow \bar{X}_e$ and $Z_e \rightarrow \bar{Z}_e$.

\mathcal{H}_G has six qubits and six stabilizer generators per unit cell (since one of the four $\bar{B}_{v,\mu}$ terms is redundant). The stabilizer

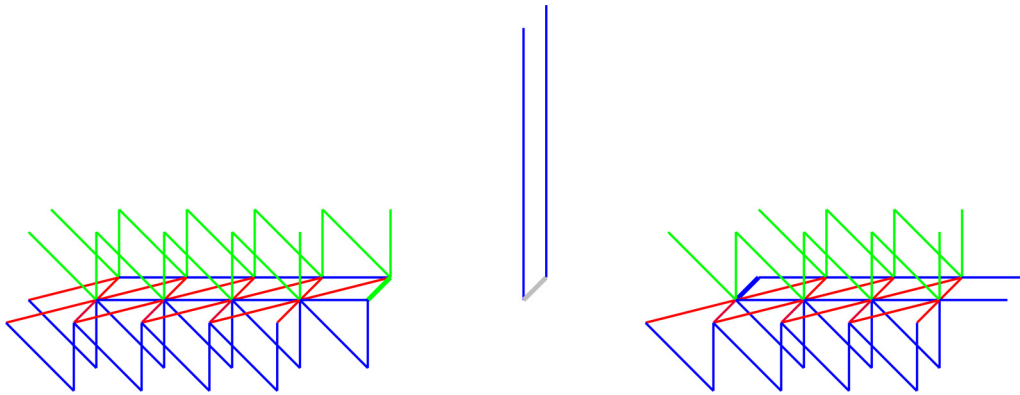


FIG. 5. Three fracton dipole string operators W_3 , W_2 , and W_1 forming a T junction (the bold edge represents the same edge in each subfigure). The fermionic exchange statistic of the fracton dipole is given by $W_3W_2^\dagger W_1W_3^\dagger W_2W_1^\dagger = -1$. The red, green, and blue edges represent Pauli operators Z , Y , and X . The bold gray edge has no Pauli action.

generators obey the following relations:

$$\prod_{c \in P} \bar{A}_c = 1, \quad \prod_{v \in P'} \bar{B}_{v,\mu} = 1, \quad (21)$$

where $c \in P$ indexes all 3-cells in a dual lattice plane P , and $v \in P'$ indexes all vertices belonging to a direct lattice plane P . However, three of these relations are redundant, hence the GSD of H_G on an $L_x \times L_y \times L_z$ lattice with periodic boundary conditions satisfies

$$\log_2 \text{GSD} = 2L_x + 2L_y + 2L_z + 2 \gcd(L_x, L_y, L_z) - 3. \quad (22)$$

The fractional excitations of H_G can be split into two sectors, which we refer to as electric charges and magnetic fluxes. The magnetic sector consists of lineons created at the endpoints of rigid string operators, which are finite segments of *wire-frame* operators equal to the product of all \bar{A}_c terms within a polyhedral region bounded by x , y , z , and w planes. Rigid string operators are equal to the product of \bar{X}_e operators over all edges of the string, which follows from the first expression of Eqs. (18). There are six species of lineons, corresponding to the six orientations of edges in the tetrahedral-octahedral honeycomb: x , y , z , $(1, -1, 0)$, $(0, 1, -1)$, and $(-1, 0, 1)$. Triples of lineons meeting at a single vertex fuse into the vacuum if their string operators belong to the corner of a wireframe operator. For example, x , y , z , and $(1, -1, 0)$, $(0, 1, -1)$, z lineon triples fuse into the vacuum, whereas x , y , $(1, -1, 0)$, and x , y , $(-1, 0, 1)$ triples do not. Due to these triple fusion rules, composite excitations of two adjacent parallel lineons, i.e., lineon dipoles, are planons. There are four species of lineon dipoles in the model: those mobile in planes normal to the x , y , z , or w directions. The loop operators for lineon dipoles are wire-frame operators with a slab geometry.

The electric sector consists of fractons created at the corners of dual lattice membrane operators composed of a product of \bar{Z}_e operators over all dual lattice faces comprising the membrane (each dual lattice face corresponds to a direct lattice edge e). Each fracton excitation is associated with a 3-cell of the tetrahedral-octahedral honeycomb. Fracton dipoles composed of a tetrahedral fracton and an adjacent octahedral fracton, are planons. There are four species of fracton dipoles

in the model: those mobile in planes normal to the x , y , z , or w directions.

The charge and flux sectors of H_G interact via generalized long-range Aharonov-Bohm statistical interactions. In particular, a phase of -1 is obtained when a lineon dipole flux encircles a fractonic charge, and likewise when a fracton dipole charge encircles a lineonic flux. These interactions arise from the commutation relations of Eqs. (19).

There are also nontrivial statistical interactions within both the electric and magnetic sectors, due to the nontrivial commutation relations of Eqs. (20). In the electric sector, the tetrahedral fractons are fermionic, whereas the octahedral fractons are bosonic. Therefore, each of the fracton dipoles is a fermion. This self-exchange statistic can be explicitly computed using the formula $\theta = W_3W_2^\dagger W_1W_3^\dagger W_2W_1^\dagger$, where W_i are three fracton dipole string operators with a common endpoint [66,67], as in Fig. 5.

In the magnetic sector, the lineons exhibit nontrivial exchange statistics and nontrivial braiding statistics with other lineons. In particular, any pair of lineons intersecting in an x , y , z , or w plane has a mutual π braiding statistic, arising from the anticommutation of intersecting lineon string operators. This can be observed from the form of the wire-frame operators, an example of which is shown in Fig. 6. As a result, lineon dipoles in adjacent planes likewise have a π braiding statistic. Moreover, each lineon dipole is a fermion.

D. Mapping to the Chamon model

We now describe a gLU transformation that maps the ground space of H_G to that of the Chamon model H_C . Based on the expressions Eqs. (3) and (22) for the GSD of these models, it is clear that for this transformation to work, a unit cell of H_G must correspond to a $2 \times 2 \times 2$ cell of H_C . Therefore, in this section, we place the Chamon model qubits on the sites of a cubic lattice with *half-integer* coordinates. With respect to the integer cubic lattice, the Chamon model has eight qubits and eight stabilizer generators per unit cell, forming a Hilbert space \mathcal{H}_C as shown in Fig. 7. We label the qubits with a double subscript v, i with $i = 1, \dots, 8$ and v the vertex of the integer lattice coinciding with qubit 1.

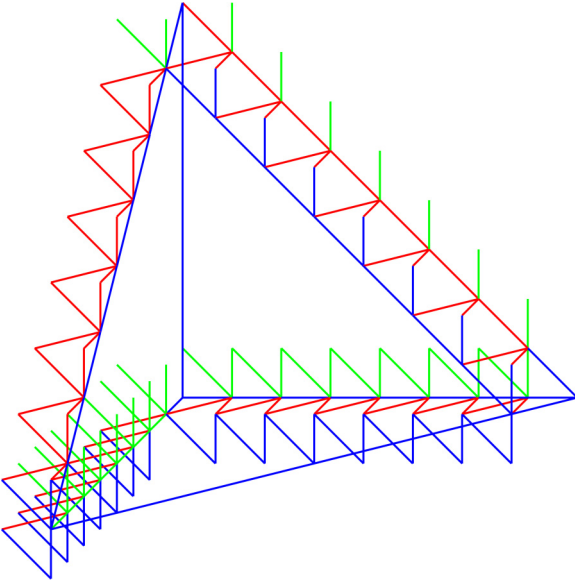


FIG. 6. A tetrahedral wireframe operator for H_G , given by a product of \widehat{A}_c terms over 3-cells inside the tetrahedron. The red, green, and blue edges represent Pauli operators Z , Y , and X .

On the other hand, the gauged model H_G has only six qubits per unit cell (one per edge of the tetrahedral-octahedral honeycomb). To match the degrees of freedom, we add two ancillary qubits per unit cell to the Hilbert space of H_G , forming a Hilbert space \mathcal{H}_G which has eight qubits per unit cell and can thus be identified with \mathcal{H}_C . Each of the eight qubits is likewise labeled with a double subscript v, i with $i = 1, \dots, 8$. Qubits 1 through 6 are those associated with the edges emanating from v in the $x, y, z, (0, 1, -1), (-1, 0, 1),$ and $(1, -1, 0)$ directions, respectively, and 7 and 8 are the two ancillary qubits. We also add two additional terms $\widehat{Z}_{v,7} \equiv Z_{v,7}$ and $\widehat{Z}_{v,8} \equiv Z_{v,8}$ for each vertex v to H_G , defining an augmented Hamiltonian H'_G .

To facilitate the transformation, in Fig. 4 we define operators $\widehat{X}_{v,i}$ and $\widehat{Z}_{v,i}$ on \mathcal{H}_C that obey relations identical to $\overline{X}_{v,i}$ and $\overline{Z}_{v,i}$ for $i = 1, \dots, 8$:

$$\begin{aligned} [[\widehat{X}_{v,i}, \widehat{X}_{v',j}]] &= [[\overline{X}_{v,i}, \overline{X}_{v',j}]], \\ \widehat{X}_{v,i}^2 = \widehat{Z}_{v,i}^2 &= 1, \quad [[\widehat{X}_{v,i}, \widehat{Z}_{v',j}]] = [[\overline{X}_{v,i}, \overline{Z}_{v',j}]], \quad (23) \\ [[\widehat{Z}_{v,i}, \widehat{Z}_{v',j}]] &= [[\overline{Z}_{v,i}, \overline{Z}_{v',j}]]. \end{aligned}$$

where $[[A, B]] \equiv A^{-1}B^{-1}AB$. (Each of these group commutators is a ± 1 phase). Due to these relations, and the fact that $\overline{Z}_{v,i}$ and $\overline{X}_{v,i}$ generate the operator algebra of \mathcal{H}_G , it follows

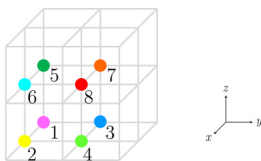


FIG. 7. A $2 \times 2 \times 2$ cell of the Chamon model, regarded as a unit cell in the transformation between H_C and H_G . There are eight qubits in the unit cell, each represented by a dot of a distinct color.

that there exists an operator algebra automorphism V mapping

$$\overline{X}_{v,i} \rightarrow \widehat{X}_{v,i}, \quad \overline{Z}_{v,i} \rightarrow \widehat{Z}_{v,i}. \quad (24)$$

Moreover, as shown in Fig. 4, V maps the terms of H'_G to a set of stabilizers

$$\{\widehat{A}_r, \widehat{A}_r', \widehat{A}_o, \widehat{B}_{v,x}, \widehat{B}_{v,y}, \widehat{B}_{v,z}, \widehat{Z}_{v,7}, \widehat{Z}_{v,8}\} \quad (25)$$

that generates the stabilizer group of H_C . Therefore,

$$VH'_G V^\dagger \sim H_C, \quad (26)$$

where \sim denotes equality of ground spaces. In the Supplemental Material (SM) MATHEMATICA file [68], we demonstrate that V is in fact a finite-depth Clifford circuit. Thus, we have arrived at the first main result of the paper: the Chamon model H_C is gLU equivalent to the gauged Hamiltonian H_G . Appendix B provides an alternative description of this transformation in terms of the polynomial description of translation invariant Pauli stabilizer codes.

To better understand this equivalence, we consider how the transformation acts on the fractional excitation superselection sectors. First, we note that the wire-frame operators of H_G are mapped by V into wire-frame operators (with even-length edges) of the Chamon model H_C . Therefore, the lineons of H_G become the lineons of H_C (with even lattice coordinates) under the transformation. This is consistent with the fact that both models exhibit a mutual π braiding statistic between intersecting lineons sharing an $x, y, z,$ or w plane. Second, we note that the loop operators for fracton dipoles of H_G are transformed into loop operators for the elementary planons of the Chamon model lying in even dual lattice planes. In other words, adjacent fracton dipoles are mapped into pairs of elementary planons of H_C separated by two lattice spacings. This is consistent with the fact that the fracton dipoles of H_G have fermionic exchange statistics but trivial mutual braiding statistics, as the elementary planons in the Chamon model are fermions that braid nontrivially with their nearest neighbors only.

E. Weak SSPT

In this section, based on the excitation content of H_G , we argue that the matter Hamiltonian H_M represents a weak SSPT state. A weak SSPT is defined as one that can be obtained by stacking 2D SPTs onto a trivial state in such a way that all planar symmetries are preserved [63,64]. In the presence of fermionic degrees of freedom, this definition can be extended to allow for stacking of noninvertible 2D topological states. In particular, we consider starting with a completely trivial state (Ising paramagnet plus atomic insulator) on the matter Hilbert space of H_M . We then stack alternating layers of invertible topological orders corresponding to the $\nu = 4$ and $\nu = -4$ states of the Kitaev 16-fold way [66] onto each plane of the tetrahedral-octahedral honeycomb. Finally, each of the S_P symmetry generators is modified such that it is the product of the original S_P with the total fermion parities of the two Kitaev states adjacent to P . It is easy to see that this modification preserves all the relations of the symmetry group. We conjecture that this state belongs to the same universality class as the model H_M .

To see why this is reasonable, it is helpful to consider the same construction on the gauged level, which should yield a model gLU equivalent to the Chamon model. In the gauged system, the stacking of Kitaev states is equivalent to stacking alternating layers of fermion parity-gauged $\nu = 4$ and $\nu = -4$ states, i.e., semion-fermion and anti-semion-fermion topological orders, onto an untwisted fermionic gauge theory (equivalent to the model described by polynomial matrix $T\Sigma$ of Appendix A). After stacking, bound states of the emergent fermion and the fracton dipole living in the same plane are condensed, confining all of the original lineons in the model but leaving deconfined bound states formed out of a lineon fused with the a semion (or antiseimion) in each of the two parallel planes. This step is equivalent to modifying the symmetry generators S_P on the ungauged level. It is clear that this procedure results in the correct braiding statistics of gauge flux planons, i.e., a mutual semionic statistic between adjacent lineon dipoles. Each of these bound-state lineons can be mapped to a (possibly dyonic) lineon of the Chamon model, therefore the condensed model has the same fractional excitation content as the Chamon model.

IV. FOLIATED FRACTON ORDER

A model is said to have FFO if its system size can be systematically reduced by disentangling, or *exfoliating*, layers of 2D topological orders from the bulk system via gLU transformation [54]. If there are n different orientations of such 2D states, the model is said to have an n -foliation structure. The first known example of FFO was the X-cube model, which has a 3-foliation structure, followed by a handful of other examples including 1-, 2-, and 3-foliated models [55–57,69].

In this section, we demonstrate that the Chamon model hosts 4-FFO, with foliation layers normal to the x, y, z , and $w = (1, 1, 1)$ directions. In particular, we show that the system size can be decreased by a constant factor m by exfoliating stacks of 2D toric codes [5] in four directions from the bulk system, where m is any odd integer. This result is consistent with previous studies on entanglement signatures [70] and compactification [71] of the model.

H_C is defined on a cubic lattice, which we will take to have integer coordinates in this section and refer to as Λ . The combination of Hamiltonian and its underlying lattice is denoted $H_C(\Lambda)$. We also define coarse-grained cubic lattices $m\Lambda$ whose lattice constants are the integer m . For a given odd m , we posit the existence of a Clifford circuit U satisfying

$$UH_C(\Lambda)U^\dagger \sim H_C(m\Lambda) + H_{2D}(m\Lambda), \quad (27)$$

where \sim denotes equality of ground spaces, and the Hamiltonian H_{2D} describes four stacks of decoupled 2D toric codes normal to the x, y, z , and w directions, respectively, each with $\frac{m-1}{2}$ toric codes per lattice spacing. We construct such a circuit explicitly in the SM MATHEMATICA file in the $m = 3, 5$ cases. In the case of general m , we show in Appendix C that unitary U exists, although we do not explicitly equate the model $H_{2D}(m\Lambda)$ to stacks of toric codes. In the following discussion, we explain the Chamon model's foliation structure (27) at the level of its fractional excitations.

In general, gapped long-range entangled phases are characterized by the structure of fractional excitations above the ground state. In FFOs, exfoliation of a set of 2D topological states corresponds to a factorization of the fusion group A of quasiparticle superselection sectors into two subgroups $A' \boxtimes A_{2D}$. Here, we use \boxtimes to denote a product of fusion groups such that there are no nontrivial mutual statistics between the two factors. A' is the fusion group of the coarse-grained fracton order, and A_{2D} is the fusion group of planons in the exfoliated topological layers.

In the case of the Chamon model, we find that the fusion group $A_C(\Lambda)$ on lattice Λ obeys the following property:

$$A_C(\Lambda) \cong A_C(m\Lambda) \boxtimes A_{2D}(m\Lambda), \quad (28)$$

where

$$A_{2D} = A_{2D}^x \boxtimes A_{2D}^y \boxtimes A_{2D}^z \boxtimes A_{2D}^w \quad (29)$$

and $A_{2D}^x, A_{2D}^y, A_{2D}^z$, and A_{2D}^w are the fusion groups of stacks of 2D toric codes in the x, y, z , and w directions, respectively, each with $\frac{m-1}{2}$ toric codes per lattice spacing. Here \cong denotes a locality-preserving isomorphism.

To see this, note that by the transformation of the previous section, the fusion rules of $H_C(\Lambda)$ are identical to those of the 4-foliated X-cube model $H_{4XC}(2\Lambda)$ discussed in Appendix A (since H_C is gLU equivalent to H_G whose fusion rules are the same as H_{4XC}). The fusion group of H_{4XC} is known to have the form $A_{4XC} = Q_{4XC} \times P_{4XC}$, where P_{4XC} is the subgroup consisting of all planon excitations [69] and Q_{4XC} is a (nonunique) finite subgroup generated by one fracton and three lineons. As an aside, this observation forms the basis of the notion of *quotient superselection sectors* (QSSs), which are defined as equivalence classes of superselection sectors modulo planons [69]. According to this definition, the group of QSS of H_{4XC} (and hence of H_C) is $A_{4XC}/P_{4XC} \cong Q_{4XC}$.

Hence, we have that $A_C = Q_C \times P_C$, where Q_C is an order-16 subgroup and $P_C = P_C^x \boxtimes P_C^y \boxtimes P_C^z \boxtimes P_C^w$ is the subgroup of all planons. The decomposition of Eq. (28) is implied by the following decomposition of P :

$$P_C(\Lambda) \cong P_C(m\Lambda) \boxtimes A_{2D}(m\Lambda), \quad (30)$$

since Q_C can always be chosen such that Q_C and $A_{2D}(m\Lambda)$ have no nontrivial mutual statistics, i.e.,

$$A_C(\Lambda) \cong [Q_C \times P_C(m\Lambda)] \boxtimes A_{2D}(m\Lambda). \quad (31)$$

The equivalence Eq. (30) can in turn be factored by direction:

$$P_C^\mu(\Lambda) \cong P_C^\mu(m\Lambda) \boxtimes A_{2D}^\mu(m\Lambda). \quad (32)$$

Thus, we can focus on the group of planons in a single direction, $P_C^\mu(\Lambda)$. Recall from Sec. II that for a given direction, there is one independent planon per lattice spacing whose loop operator is given by the product of O_c terms in a particular dual lattice plane. The total group is generated by the set of all such elementary planons. Each elementary planon has fermionic exchange statistics. Moreover, neighboring planons have mutual semionic braiding statistics.

To demonstrate Eq. (30), we need to find an alternative set of generating planons that splits into two parts: one that generates $P_C^\mu(m\Lambda)$ and one that generates $A_{2D}^\mu(m\Lambda)$. Actually,

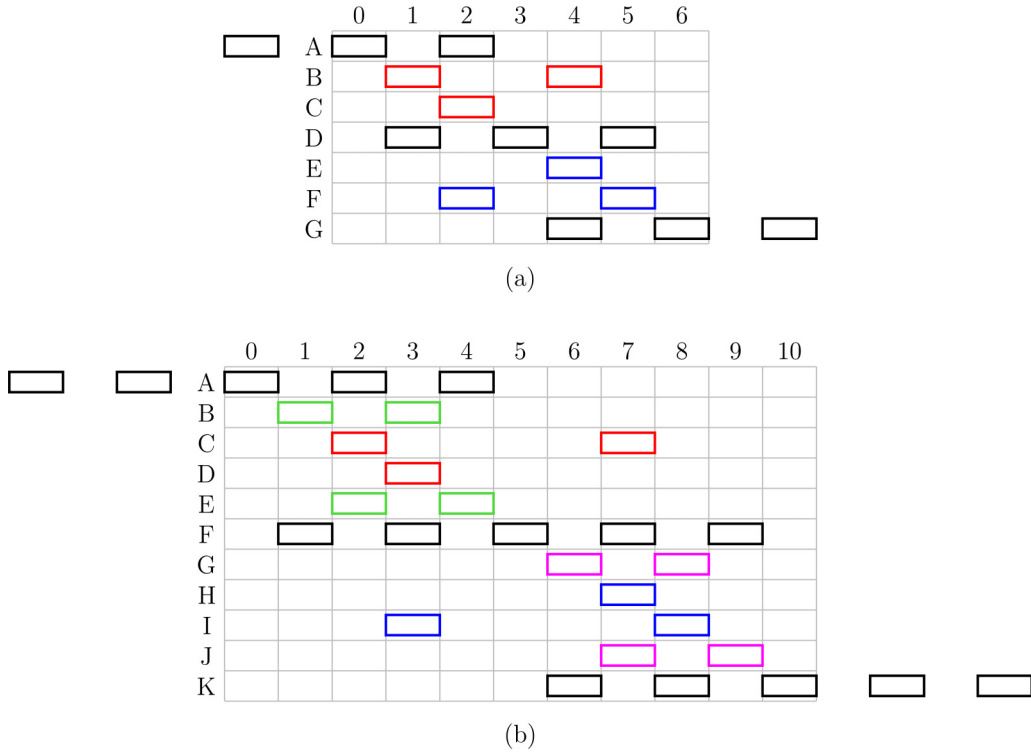


FIG. 8. Planon diagrams depicting coarse-grained bases of μ -normal planons in a given direction $\mu = x, y, z, w$ for the (a) $m = 3$ and (b) $m = 5$ cases. Each basis is translation-invariant with respect to the enlarged unit cell of $2m\Lambda$. Each vertical line is commensurate with a μ -normal lattice plane, hence the numbers 0 to $2m$ represent dual lattice coordinates. A box lying in column k represents a planon living in that dual lattice plane. On the other hand, each horizontal row represents a single generator of our chosen basis, equal to the fusion product of all elementary planons in the row. Since each unit cell contains $2m$ basis planons, A and G (K) belong to different unit cells for the $m = 3$ ($m = 5$) case. The planon bases are partitioned into m subsets of two generators per unit cell, such that they have pairwise trivial mutual braiding statistics. (Recall that adjacent planons of the Chamon model have a mutual π braiding statistic.) For $m = 3$, the subsets are colored black (ADG), red (BC), and blue (EF), whereas for $m = 5$ they are colored black (AFK), green (BE), red (CD), purple (GJ), and blue (HI). The black planons are excitations of the coarse-grained Chamon model $H_C(m\Lambda)$, as they are fermions (being composed of an odd number of fermions with trivial mutual statistics) with a mutual π braiding statistic between adjacent pairs. On the other hand, each of the remaining $m - 1$ pairs of planons generates a decoupled layer of 2D toric code. These diagrams verify the relation (33).

we will show the following equivalent relation:¹

$$P_C^\mu(\Lambda) \cong P_C^\mu(m\Lambda) \boxtimes A_{2D}^\mu(2m\Lambda) \boxtimes A_{2D}^\mu(2m\Lambda). \quad (33)$$

Factorization of this form for $m = 3$ and $m = 5$ are depicted in the planon diagrams of Fig. 8, demonstrating that the fractional excitation structure of H_C indeed exhibits the decomposition of Eq. (28). It is straightforward to generalize these diagrams for larger m . Thus, we conclude that the Chamon model exhibits a 4-foliation structure of 2D toric code layers in the x, y, z , and w directions.

V. DISCUSSION

In this paper, we have carried out a comprehensive investigation of the Chamon model. Specifically, we have demonstrated two results: First, its characterization as a twisted 4-foliated gauge theory with emergent fermionic

charge. Second, we have found that it has a 4-foliation structure composed of 2D toric code layers. The foliation structure is consistent with a conjecture of Ref. [61], which outlines conditions under which a copy of 2D toric code can be extracted from a 3D stabilizer code model under a local unitary. The emergent gauge theory structure found in this paper has been used by two of the authors to write a topological defect network for the Chamon model [72].

The transformation between the Chamon model and the 4-foliated X-cube variant H_G is reminiscent of previous findings about the checkerboard model [55] and the Majorana checkerboard model [8], which were, respectively, shown to be equivalent to two copies of the (3-foliated) X-cube model and to the semionic X-cube model [56] (plus transparent fermions), each of which has a clear gauge theory description. It is similarly reminiscent of the equivalence between the Wen plaquette model [59] and the 2D toric code [66]. These transformations all have in common that the original model, e.g., Chamon, has an enhanced translation symmetry compared with the transformed model, e.g., H_G . Therefore, the respective gauge theory descriptions are enriched by translation symmetry via a nontrivial permutation on the fractonic

¹The additional coarse-graining by a factor of two is necessary to pair up 3-fermion states so they can be transformed into pairs of toric codes.

superselection sectors. We leave a detailed exploration of this topic to future studies.

While it is known that CSS stabilizer codes can generically be characterized via emergent gauge theory, our results raise the question of how generally non-CSS codes in three dimensions admit such a description. It seems plausible that all stabilizer codes possess a gauge theory description and hence it could be enlightening to study more examples. For instance, one could check whether a gauge theory description, analogous to the Chamon model, is possible for the fracton models in Ref. [29]. Another question raised by this paper is that of strong subsystem symmetry-protected topological (SPT) states in fermionic systems, whose classification is an open problem. We have argued that the Chamon model is dual to a weak subsystem SPT.

More generally, it is an open question to what extent the framework of emergent gauge theory has utility in the classification of fractonic phases of matter. To our knowledge, among the class of exactly solvable lattice models, there are no examples that are explicitly known to not admit a gauge theory description. It would be interesting to either find such an example or demonstrate that none exist. On the other hand, there are examples of fractonic orders with excitations of infinite order which are unlikely to have any characterization in terms of finite gauge groups (although they arise naturally as infinite-component $U(1)$ Chern-Simons gauge theories [73]).

Finally, it is worthwhile to note that some of the fractonic excitations in the Chamon model exhibit nonbosonic self-exchange statistics [74]. For the present analysis, it has been sufficient to consider in detail the statistics of planon excitations. A systematic investigation of fracton self-statistics in n -foliated models is left to future work.

ACKNOWLEDGMENTS

W.S. is grateful to Xie Chen and Kevin Slagle for many inspiring discussions. A.D. thanks Dominic J. Williamson for related discussions. W.S. and A.D. are supported by the Simons Foundation through the collaboration on Ultra-Quantum Matter (No. 651444, W.S.; No. 651438, A.D.) and by the Institute for Quantum Information and Matter, an NSF Physics Frontiers Center (No. PHY-1733907). W.S. also received support from the National Science Foundation under the Award No. DMR-1654340.

APPENDIX A: RELATION BETWEEN H_G AND THE 4-FOLIATED X-CUBE MODEL

In this Appendix, we introduce the 4-foliated X-cube model H_{4XC} and describe its relation to H_G . The fusion

structure of excitations of H_{4XC} is identical to that of H_G . However, the models differ in terms of the self- and mutual statistics of the excitations. In this Appendix, we will use the $\mathbb{Z}_2[x, y, z, 1/x, 1/y, 1/z]$ Laurent polynomial ring formalism for describing translation-invariant Pauli stabilizer codes [15]. In this formalism, Pauli operators in a cubic lattice system with n qubits per site are represented by length $2n$ column vectors whose entries are elements of $\mathbb{Z}_2[x, y, z, 1/x, 1/y, 1/z]$. The first n entries represent the Pauli X components, and the last n entries the Pauli Z components.

The Hilbert space of H_{4XC} is the same as that of H_G . It is composed of one qubit on each edge of the tetrahedral-octahedral honeycomb. The Hamiltonian has the form

$$H_{4XC} = - \sum_c A_c - \sum_{v,\mu} B_{v,\mu}, \quad (A1)$$

where c runs over all 3-cells of the honeycomb, v all vertices, $\mu = x, y, z, w$, and

$$A_c = \prod_{e \in c} X_e, \quad B_{v,\mu} = \prod_{v \ni e \perp \mu} Z_e. \quad (A2)$$

The terms are shown in Fig. 9. This model is described by the polynomial matrix

$$\Sigma = \begin{pmatrix} A & 0 \\ 0 & B \end{pmatrix}, \quad (A3)$$

where

$$A = \begin{pmatrix} 1 & yz & y+z \\ 1 & zx & z+x \\ 1 & xy & x+y \\ 1 & x & x+1 \\ 1 & y & y+1 \\ 1 & z & z+1 \end{pmatrix}, \quad B = \begin{pmatrix} 0 & 1+\frac{1}{x} & 1+\frac{1}{x} \\ 1+\frac{1}{y} & 0 & 1+\frac{1}{y} \\ 1+\frac{1}{z} & 1+\frac{1}{z} & 0 \\ \frac{1}{y}+\frac{1}{z} & 0 & 0 \\ 0 & \frac{1}{x}+\frac{1}{z} & 0 \\ 0 & 0 & \frac{1}{x}+\frac{1}{y} \end{pmatrix}. \quad (A4)$$

The columns of A represent the 3-cell terms $A_t, A_{t'}$, and A_o , whereas the columns of B represent the vertex terms $B_{v,x}, B_{v,y}$, and $B_{v,z}$, which together generate $B_{v,w}$. Note that $\Sigma^\dagger \Omega_6 \Sigma = 0$, where \dagger represents transposition combined with spatial inversion, $\Omega_k = \begin{pmatrix} 0 & I_k \\ I_k & 0 \end{pmatrix}$ is the $2k \times 2k$ symplectic form, and

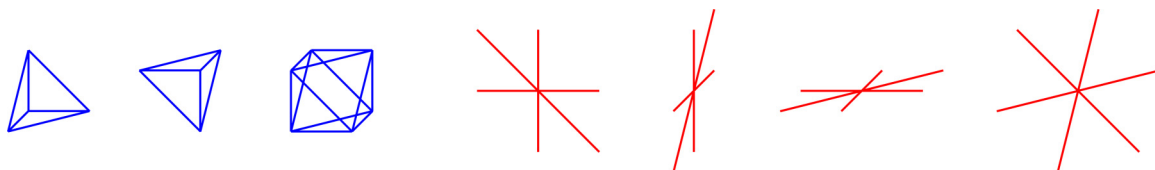


FIG. 9. The terms $A_t, A_{t'}, A_o, B_{v,x}, B_{v,y}, B_{v,z}$, and $B_{v,w}$ of H_{4XC} , where t and t' are oppositely oriented tetrahedral cells and o an octahedral cell. Here blue represents Pauli X and red Pauli Z. Each term is a tensor product of the depicted Pauli operators.

I_k the $k \times k$ identity matrix. Thus, the terms of H_{4XC} are mutually commuting.

H_G can be obtained from H_{4XC} via a pair of locality-preserving, invertible but nonisomorphic transformations of the Pauli group \mathcal{P} :

$$W : \mathcal{P} \rightarrow \mathcal{P}, \quad T : \mathcal{P} \rightarrow \mathcal{P}. \quad (\text{A5})$$

In the polynomial formalism, these transformations correspond to multiplication by invertible but nonsymplectic matrices:

$$W = \begin{pmatrix} I_6 & 0 \\ \tilde{W} & I_6 \end{pmatrix}, \quad T = \begin{pmatrix} I_6 & \tilde{T} \\ 0 & I_6 \end{pmatrix}, \quad (\text{A6})$$

where

$$\tilde{W} = \begin{pmatrix} 1 & 1 & 0 & z & z & 0 \\ 0 & 0 & 0 & 0 & 0 & 0 \\ 1 & 1 & 0 & z & z & 0 \\ \frac{1}{y} & \frac{1}{y} & 0 & \frac{z}{y} & \frac{z}{y} & 0 \\ 0 & 0 & 0 & 0 & 0 & 0 \\ \frac{1}{y} & \frac{1}{y} & 0 & \frac{z}{y} & \frac{z}{y} & 0 \end{pmatrix},$$

$$\tilde{T} = \begin{pmatrix} 0 & 1 + \frac{y}{x} & 0 & 0 & z + 1 & 0 \\ 0 & 0 & 0 & 0 & 0 & 0 \\ 1 + \frac{x}{z} & 1 + \frac{y}{z} & 0 & 0 & x + 1 & 0 \\ 1 + \frac{x}{yz} & 1 + \frac{1}{z} & 1 + \frac{1}{y} & 0 & 1 + \frac{x}{y} & 0 \\ 0 & 1 + \frac{y}{xz} & 0 & 0 & 0 & 0 \\ 1 + \frac{1}{y} & 1 + \frac{1}{x} & 1 + \frac{z}{xy} & 1 + \frac{z}{x} & 1 + \frac{z}{y} & 0 \end{pmatrix}. \quad (\text{A7})$$

Note that $T^2 = W^2 = 1$. It holds that

$$\bar{A}_c = T(W(A_c)), \quad \bar{B}_{v,\mu} = T(W(B_{v,\mu})). \quad (\text{A8})$$

Therefore, the Hamiltonian H_G is represented by the polynomial matrix $\bar{\Sigma} = TW\Sigma$. Since $\bar{\Sigma}^\dagger \Omega_6 \bar{\Sigma} = 0$, the terms of H_G mutually commute hence defining a stabilizer code. Note that

$$TW = \begin{pmatrix} I_6 + \tilde{T}\tilde{W} & \tilde{T} \\ \tilde{W} & I_6 \end{pmatrix}. \quad (\text{A9})$$

The T and W transformations can also be used to define two other non-CSS stabilizer code Hamiltonians, represented by the polynomial matrices $W\Sigma$ and $T\Sigma$, satisfying $\Sigma^\dagger W^\dagger \Omega_6 W \Sigma = 0$ and $\Sigma^\dagger T^\dagger \Omega_6 T \Sigma = 0$. The Hamiltonians represented by Σ , $\bar{\Sigma}$, $W\Sigma$, and $T\Sigma$ can each be obtained via a gauging procedure of four stacks of planar \mathbb{Z}_2 symmetries. The procedure was described explicitly for H_G , represented by $\bar{\Sigma}$, in Sec. III B. On the other hand, Σ , $W\Sigma$, and $T\Sigma$ can be obtained by gauging the following matter Hamiltonians, respectively:

$$H_M^{(1)} = - \sum_t X_t - \sum_o X_o, \quad (\text{A10})$$

$$H_M^{(2)} = - \sum_t X_t - \sum_o X_o, \quad (\text{A11})$$

$$H_M^{(3)} = - \sum_t i\gamma_t \gamma'_t - \sum_o X_o. \quad (\text{A12})$$

The Hilbert space of $H_M^{(3)}$ is the same as that of H_M , whereas those of $H_M^{(1)}$ and $H_M^{(2)}$ differ in that the fermionic orbital on

each tetrahedral 3-cell is replaced by a qubit. The symmetries of $H_M^{(3)}$ are the same as those of H_M , whereas for $H_M^{(1)}$ and $H_M^{(2)}$ they are simply a product of Pauli X operators over all 3-cells in a given dual lattice plane.

Therefore, each of the models Σ , $\bar{\Sigma}$, $W\Sigma$, and $T\Sigma$ represents a distinct kind of fractonic gauge theory. Σ is coupled to a trivial bosonic paramagnet, $T\Sigma$ to a trivial atomic insulator/paramagnet state, $W\Sigma$ to a bosonic SSPT state, and $\bar{\Sigma}$ to a fermionic SSPT. The fusion rules of all four models are identical; moreover, the generalized Aharonov-Bohm statistics between gauge charge and flux sectors have identical form. However, the models differ in terms of the statistics *within* the charge and flux sectors. Acting on Σ , the W matrix represents a *twist* of the gauge flux statistics, whereas the T matrix represents a *transmutation* of the gauge charge statistics. This can be seen from the equations

$$W^\dagger \Omega_6 W = \begin{pmatrix} \tilde{W} + \tilde{W}^\dagger & I_6 \\ I_6 & 0 \end{pmatrix},$$

$$T^\dagger \Omega_6 T = \begin{pmatrix} 0 & I_6 \\ I_6 & \tilde{T} + \tilde{T}^\dagger \end{pmatrix},$$

$$W^\dagger T^\dagger \Omega_6 T W = \begin{pmatrix} \tilde{W} + \tilde{W}^\dagger & I_6 \\ I_6 & \tilde{T} + \tilde{T}^\dagger \end{pmatrix}. \quad (\text{A13})$$

The off-diagonal components represent the Aharonov-Bohm interactions whereas the diagonal components represent the statistics within the charge and flux sectors. Therefore, Σ and $W\Sigma$ have purely bosonic gauge charge statistics, whereas the tetrahedral fractonic charges of $\bar{\Sigma}$ and $T\Sigma$ are fermionic. On the other hand, Σ and $W\Sigma$ have purely bosonic gauge flux lineons, whereas intersecting lineons of $\bar{\Sigma}$ and $W\Sigma$ have a mutual semionic braiding statistic.

APPENDIX B: POLYNOMIAL REPRESENTATION OF THE TRANSFORMATION FROM H_G TO H_C

In this Appendix, we express the transformation from the gauge theory Hamiltonian H_G to the Chamon model H_C in terms of the Laurent polynomial formalism. Regarding a $2 \times 2 \times 2$ cell as the unit cell with qubits labeled as in Fig. 7, H_C is represented by the 16×8 stabilizer map:

$$\hat{\Sigma} = \begin{pmatrix} 0 & x & y & 0 & 0 & xz & yz & 0 \\ 1 & 0 & 0 & y & z & 0 & 0 & yz \\ 1 & 0 & 0 & x & z & 0 & 0 & xz \\ 0 & 1 & 1 & 0 & 0 & z & z & 0 \\ 0 & x & y & 0 & 0 & x & y & 0 \\ 1 & 0 & 0 & y & 1 & 0 & 0 & y \\ 1 & 0 & 0 & x & 1 & 0 & 0 & x \\ 0 & 1 & 1 & 0 & 0 & 1 & 1 & 0 \\ 0 & 0 & y & xy & z & xz & 0 & 0 \\ 0 & 0 & y & y & z & z & 0 & 0 \\ 1 & x & 0 & 0 & 0 & 0 & z & xz \\ 1 & 1 & 0 & 0 & 0 & 0 & z & z \\ 1 & x & 0 & 0 & 0 & 0 & y & xy \\ 1 & 1 & 0 & 0 & 0 & 0 & y & y \\ 0 & 0 & 1 & x & 1 & x & 0 & 0 \\ 0 & 0 & 1 & 1 & 1 & 1 & 0 & 0 \end{pmatrix}. \quad (\text{B1})$$

We define a matrix C whose first (last) eight columns represent the operators $\widehat{X}_{v,i}$ ($\widehat{Z}_{v,i}$) for $i = 1, \dots, 8$:

$$C = \begin{pmatrix} 1 & 1 & 0 & z & z & 0 & 0 & 1 & 0 & 0 & 0 & 0 & 0 & 0 & 1 & 0 \\ 1 & 0 & 0 & 0 & 0 & 0 & 0 & 1 & 0 & 1 + \frac{y}{x} & \frac{z}{x} & \frac{yz}{x} & z & y & 0 & 0 \\ 0 & 1 & 0 & 0 & 0 & 0 & 0 & 0 & 0 & 0 & \frac{z}{y} & z & \frac{xz}{y} & 0 & 0 & 1 + \frac{x}{y} \\ 0 & 0 & 0 & 0 & 0 & 0 & 0 & \frac{1}{y} & 0 & 0 & 0 & 0 & 0 & 1 & \frac{1}{y} & 0 \\ 0 & 0 & 0 & 0 & 0 & 0 & 0 & 1 & 0 & 0 & 1 & 0 & 0 & 0 & 1 & 0 \\ 0 & 0 & 0 & 1 & 0 & 0 & 0 & \frac{1}{y} & 1 & 1 & 1 & 0 & 1 + \frac{x}{y} & 1 & 0 & \frac{1}{z} + \frac{x}{yz} \\ 0 & 0 & 0 & 0 & 0 & 0 & 0 & 0 & 0 & 0 & \frac{1}{y} & 0 & 0 & 1 & \frac{1}{y} & 0 \\ 0 & 1 & 1 & y+z & z & y & 0 & 1 & 0 & 0 & 0 & 0 & 0 & 0 & 1 & 1 \\ 0 & 0 & 0 & 0 & 0 & 0 & 0 & 1 & 1 & 0 & 0 & 0 & 0 & 0 & 1 & 1 \\ 0 & 1 & 0 & 0 & 0 & 0 & 0 & 0 & 0 & 1 & \frac{z}{y} & z & \frac{xz}{y} & 0 & 0 & \frac{x}{y} \\ 0 & 0 & 0 & 0 & 0 & 1 & \frac{1}{y} & \frac{1}{y} & 1 + \frac{1}{y} & 1 + \frac{1}{x} & 1 + \frac{z}{xy} & 1 + \frac{z}{x} & 1 + \frac{z}{y} & 1 & 0 & \frac{x}{y} \\ 0 & 0 & 1 & 0 & 0 & 0 & 1 & 1 & 0 & 1 & 1 & 0 & x & 0 & 0 & \frac{x}{z} \\ 0 & 0 & 0 & 0 & 1 & 0 & 0 & 0 & 1 & 1 & 1 & 0 & 1 & 0 & 0 & \frac{1}{z} \\ 0 & 0 & 0 & 0 & 0 & 0 & 0 & \frac{1}{y} & 0 & 0 & 0 & 1 & 0 & 0 & \frac{1}{y} & \frac{1}{z} \\ 0 & 0 & 0 & 0 & 0 & 0 & \frac{1}{y} & 0 & \frac{1}{y} & 0 & 0 & 1 & 0 & 0 & \frac{1}{y} & \frac{1}{z} \end{pmatrix}. \quad (\text{B2})$$

In this Appendix, we will redefine the matrices W and T from the previous Appendix such that they accommodate the two ancillary qubits. In particular,

$$W = \begin{pmatrix} I_8 & 0 \\ \widetilde{W} \oplus I_2 & I_8 \end{pmatrix}, \quad T = \begin{pmatrix} I_8 & \widetilde{T} \oplus I_2 \\ 0 & I_8 \end{pmatrix}. \quad (\text{B3})$$

Then, we define a matrix $V = CWT$ satisfying $V^\dagger \Omega_8 V = \Omega_8$ and $VTW = C$. Therefore V is a Clifford QCA that maps $\overline{X}_{v,i} \rightarrow \widehat{X}_{v,i}$ and $\overline{Z}_{v,i} \rightarrow \widehat{Z}_{v,i}$. Moreover,

$$V\overline{\Sigma} = \widehat{\Sigma}V_2, \quad (\text{B4})$$

where V_2 is the invertible matrix:

$$V_2 = \begin{pmatrix} 1 & 0 & 0 & \frac{1}{y} & 0 & \frac{1}{y} & 0 & 0 \\ 0 & 0 & 1 & 0 & 0 & \frac{1}{x} & 0 & 0 \\ 0 & 0 & 1 & \frac{1}{y} & \frac{1}{y} & \frac{1}{y} & \frac{1}{y} & 0 \\ 0 & 0 & 1 & 0 & \frac{1}{xy} & \frac{1}{xy} & 0 & 0 \\ 0 & 0 & 1 & \frac{1}{z} & 0 & 0 & 0 & \frac{1}{z} \\ 0 & 0 & 1 & 0 & 0 & 0 & 0 & 0 \\ 0 & 0 & 1 & \frac{1}{yz} & \frac{1}{yz} & 0 & 0 & 0 \\ 0 & 1 & 0 & 0 & \frac{1}{yz} & 0 & 0 & \frac{1}{yz} \end{pmatrix}. \quad (\text{B5})$$

Therefore, V maps the ground space of H_G to that of H_C . In the SM MATHEMATICA file, we demonstrate that V is actually a finite-depth Clifford circuit (i.e., it can be decomposed into a product of elementary symplectic transformations). This demonstrates that H_G and H_C are gLU equivalent.

APPENDIX C: ENTANGLEMENT RENORMALIZATION OF THE CHAMON MODEL

In this Appendix, we study the ER on the Chamon model using the polynomial formalism [15,22]. The stabilizer map σ and the excitation map ϵ for the Chamon model can be written

as

$$\sigma = \begin{pmatrix} (1+x^{-1})(y^{-1}+z^{-1}) \\ (1+y^{-1})(x^{-1}+z^{-1}) \end{pmatrix} \quad (\text{C1})$$

and

$$\epsilon = \sigma^\dagger \Omega_1 = ((1+y)(x+z)(1+x)(y+z)), \quad (\text{C2})$$

respectively [15]. Our approach to doing ER involves going to a basis of stabilizer terms such that the associated basis excitations include the bosonic planon charges. Then we write the creation operators or movers of these bosonic charges and apply translation invariant gates (up to coarse graining) to reduce them into a canonical form of unit vectors. The excitations that form the bosonic planons and the relative positions between them are shown in Fig. 8. Before stating an explicit ER result for the Chamon model, we first prove that a coarse-grained copy of itself can be extracted under ER of the Chamon model. In particular, we have the following theorem.

Theorem C.1. For any odd m , there exists a Clifford circuit U such that

$$UHC(\Lambda)U^\dagger \sim H_C(m\Lambda) + H_B(m\Lambda) \quad (\text{C3})$$

for some Pauli Hamiltonian H_B . Here \sim denotes equality of ground spaces.

Proof. We first write two fracton creation operators,

$$s_1 = x^{m-1}(1+y+\dots+y^{m-1})(1+z/x+\dots+(z/x)^{m-1})(1,0)^T$$

and

$$s_2 = y^{m-1}(1+x+\dots+x^{m-1})(1+z/y+\dots+(z/y)^{m-1})(0,1)^T,$$

which create fracton excitations at the sites corresponding to the polynomials $(1+y^m)(x^m+z^m)$ and $(1+x^m)(y^m+z^m)$, respectively. Note that s_1 and s_2 are related via permutation of x and y . In other words, the action of the excitation map as defined in Eq. (C2) on operators s_1 and s_2 is given by

$$\epsilon s_1 = (1+y^m)(x^m+z^m),$$

$$\epsilon s_2 = (1+x^m)(y^m+z^m).$$

Under coarse graining of the lattice, the translation group is reduced such that the translation variables modify to $x' = x^m$, $y' = y^m$, $z' = z^m$. On the coarse-grained lattice, the representation of the creation operators s_1 and s_2 is given by $s_1^{(m)}$ and $s_2^{(m)}$, respectively; namely, $\phi_{\#}^m(s_1) = s_1^{(m)}$ and $\phi_{\#}^m(s_2) = s_2^{(m)}$ where $\phi_{\#}^m$ is the map that implements coarse graining by a factor of m . We now state two lemmas about $s_1^{(m)}$ and $s_2^{(m)}$, one about the commutation relation and the other about reducing them to a canonical form via elementary symplectic transformations. The proofs of these lemmas are given after this proof.

Lemma C.1. For odd m , $s_1^{(m)\dagger} \Omega_m s_2^{(m)} = 1$, where $\Omega_m = \begin{pmatrix} 0 & \mathbb{1} \\ \mathbb{1} & 0 \end{pmatrix}$ is a $2m \times 2m$ symplectic form and $\mathbb{1}$ is an $m \times m$ identity matrix.

Lemma C.2. For odd m , the creation operators $s_1^{(m)}$ and $s_2^{(m)}$ can be mapped to

$$\begin{aligned} s_1^{(m)} &= (1 \quad 0 \cdots 0 \quad | \quad 0 \quad \cdots 0)^T, \\ s_2^{(m)} &= (0 \quad 0 \cdots 0 \quad | \quad 1 \quad \cdots 0)^T. \end{aligned} \quad (C4)$$

via translation invariant elementary symplectic transformations. Here, as shown, $s_1^{(m)}$ and $s_2^{(m)}$, respectively, have only one nonzero entry at the first and (m^3+1) th vector components.

The excitation represented as a singleton element, (1) before coarse-graining, is represented by the unit vector $e_1 = (1, 0, 0, \dots, 0)^T$ with m entries after coarse graining. Considering the action of ϵ on the creation operators $s_1^{(m)}$, $s_2^{(m)}$ yields $\epsilon s_1^{(m)} = (1 + y')(x' + z')e_1$ and $\epsilon s_2^{(m)} = (1 + x')(y' + z')e_1$, the excitation map becomes

$$\epsilon = \begin{pmatrix} (1+y)(x+z) & \star & \star & \cdots & \star & (1+x)(y+z) & \star & \star & \cdots & \star \\ 0 & \star & \star & \cdots & \star & 0 & \star & \star & \cdots & \star \\ \vdots & \vdots & \vdots & \vdots & \vdots & \vdots & & & & \\ 0 & \star & \star & \cdots & \star & 0 & \star & \star & \cdots & \star \end{pmatrix}, \quad (C5)$$

where we suppressed the $'$ in the coarse-grained translation variables and where \star indicates unknown entries. Since

$$((1+x^{-1})(y^{-1}+z^{-1}) \quad 0 \quad 0 \quad \cdots \quad 0 \quad (1+y^{-1})(x^{-1}+z^{-1}) \quad 0 \quad 0 \quad \cdots \quad 0)^T \in \ker \epsilon,$$

the topological order condition $\ker \epsilon = \text{im} \sigma = \text{im} \Omega_g \epsilon^\dagger$ implies that the rows of ϵ must generate

$$((1+y)(x+z) \quad 0 \quad 0 \quad \cdots \quad 0 \quad (1+x)(y+z) \quad 0 \quad 0 \quad \cdots \quad 0)^T.$$

This implies that we can insert this as a row in the excitation map as follows:

$$\epsilon = \begin{pmatrix} (1+y)(x+z) & 0 & 0 & \cdots & 0 & (1+x)(y+z) & 0 & 0 & \cdots & 0 \\ (1+y)(x+z) & \star & \star & \cdots & \star & (1+x)(y+z) & \star & \star & \cdots & \star \\ 0 & \star & \star & \cdots & \star & 0 & \star & \star & \cdots & \star \\ \vdots & \vdots & \vdots & \vdots & \vdots & \vdots & & & & \\ 0 & \star & \star & \cdots & \star & 0 & \star & \star & \cdots & \star \end{pmatrix}. \quad (C6)$$

On applying appropriate row operations, we get

$$\epsilon = \begin{pmatrix} (1+y)(x+z) & 0 & 0 & \cdots & 0 & (1+x)(y+z) & 0 & 0 & \cdots & 0 \\ 0 & \star & \star & \cdots & \star & 0 & \star & \star & \cdots & \star \\ 0 & \star & \star & \cdots & \star & 0 & \star & \star & \cdots & \star \\ \vdots & \vdots & \vdots & \vdots & \vdots & \vdots & & & & \\ 0 & \star & \star & \cdots & \star & 0 & \star & \star & \cdots & \star \end{pmatrix}. \quad (C7)$$

Thus, we have extracted a copy of the Chamon model.

We now give proofs of the two lemmas that were used in proving Theorem C.1.

Proof of Lemma C.1 The polynomial given by $s_1^\dagger \Omega_1 s_2$ encodes the commutation of translates of s_1 and s_2 . Here, $\Omega_m = \begin{pmatrix} 0 & \mathbb{1} \\ \mathbb{1} & 0 \end{pmatrix}$ is an $2m \times 2m$ symplectic form and $\mathbb{1}$ is an $m \times m$ Identity matrix. Let us denote the coefficient of g in the polynomial $s_1^\dagger \Omega_1 s_2$ as $(s_1^\dagger \Omega_1 s_2)_g$. We note that two Pauli operators a and b commute if $(a^\dagger \Omega_g b)_1 = 0$.

Note that s_1 and s_2 can be expressed as follows:

$$s_1 = (1 + y + \dots + y^{m-1})(x^{m-1} + zx^{m-2} + \dots + z^{m-1})(1, 0)^T$$

and

$$s_2 = (1 + x + \dots + x^{m-1})(y^{m-1} + zy^{m-2} + \dots + z^{m-1})(0, 1)^T.$$

Since all powers of translation variables are less than m , under coarse graining by a factor of m in each direction, we are left with $2m$ -dimensional vectors for s_1 and s_2 with only 1s and 0s. For s_1 , the 1s appear in the first half and for s_2 , in the second half. Due to this form, $s_1^{(m)\dagger} \Omega_m s_2^{(m)} = (s_1^{(m)\dagger} \Omega_m s_2^{(m)})_1$, i.e., only the coefficient of 1 contributes and there are no monomials. Since the commutation relation between the operators s_1 and

s_2 , i.e., $(s_1^\dagger \Omega_1 s_2)_1$ is not affected by coarse graining, we get

$$\begin{aligned} & s_1^{(m)\dagger} \Omega_m s_2^{(m)} \\ &= (s_1^{(m)\dagger} \Omega_m s_2^{(m)})_1 \\ &= (s_1^\dagger \Omega_1 s_2)_1 \\ &= m \pmod{2}. \end{aligned} \quad (\text{C8})$$

Thus, $s_1^{(m)\dagger} \Omega_m s_2^{(m)} = 1$ when m is odd. ■

Proof of Lemma C.2 For both s_1 and s_2 , the degrees of translation variables x , y , and z range from 0 to $m - 1$. Thus, after coarse graining, $s_1^{(m)}$ and $s_2^{(m)}$ are both supported at only one unit cell (at location 1). In particular, $s_1^{(m)}$ is a Laurent polynomial vector over $\mathbb{F}_2[1]$, satisfying $s_1^{(m)\dagger} \Omega_m s_1^{(m)} = 0$. Since $\mathbb{F}_2[1]$ is a principal ideal domain, we can find an elementary symplectic transformation E_1 composed of CNOT gates that turns s_1 into a vector with a single nonzero component, say, g at the first entry. Since the only nonzero component in $\mathbb{F}_2[1]$ is 1, $g = 1$.

Since the transformation E_1 acts only at the origin, $E_1 s_2^{(m)}$ still acts only at location 1 and thus is a Laurent polynomial vector over $\mathbb{F}_2[1]$. Since $s_1^{(m)\dagger} \Omega_m s_2^{(m)} = 1$, the $(m^3 + 1)$ th component of $E_1 s_2^{(m)}$ must be 1. Since $E_1 s_2^{(m)}$ can have nonzero entries, i.e., 1s only in the second half of the vector, they can all be cancelled out via CNOT gates without affecting the form of $s_1^{(m)}$. Thus, we get the form of $s_1^{(m)}$ and $s_2^{(m)}$ as desired.

1. Explicit ER circuit

In the SM MATHEMATICA file, we have constructed a circuit U which carries out an explicit ER of the Chamon model given as follows:

$$\begin{aligned} U H_C(\Lambda) U^\dagger &\sim H_C(3\Lambda) + H_{2D}(6\Lambda) + H_{2D}(6\Lambda), \\ H_{2D} &= H_x^{\text{toric}} + H_y^{\text{toric}} + H_z^{\text{toric}} + H_w^{\text{toric}}. \end{aligned} \quad (\text{C9})$$

Here, H_μ^{toric} is a stack of 2D toric codes along the μ direction with one layer per lattice spacing.

-
- [1] X. Chen, Z.-C. Gu, and X.-G. Wen, *Phys. Rev. B* **82**, 155138 (2010).
- [2] R. B. Laughlin, *Phys. Rev. Lett.* **50**, 1395 (1983).
- [3] X.-G. Wen, *Adv. Phys.* **44**, 405 (1995).
- [4] M. W. de Propitius and F. A. Bais, Discrete gauge theories, in *Particles and Fields*, edited by G. Semenoff and L. Vinet (Springer New York, 1999), pp. 353–439
- [5] A. Y. Kitaev, *Ann. Phys.* **303**, 2 (2003).
- [6] E. Witten, *Commun. Math. Phys.* **117**, 353 (1988).
- [7] C. Chamon, *Phys. Rev. Lett.* **94**, 040402 (2005).
- [8] S. Vijay, J. Haah, and L. Fu, *Phys. Rev. B* **92**, 235136 (2015).
- [9] S. Vijay, J. Haah, and L. Fu, *Phys. Rev. B* **94**, 235157 (2016).
- [10] P. Gorantla, H. T. Lam, N. Seiberg, and S.-H. Shao, *Phys. Rev. B* **104**, 235116 (2021).
- [11] K. Slagle and Y. B. Kim, *Phys. Rev. B* **97**, 165106 (2018).
- [12] S. Bravyi, B. Leemhuis, and B. M. Terhal, *Ann. Phys.* **326**, 839 (2011).
- [13] J. Haah, *Phys. Rev. A* **83**, 042330 (2011).
- [14] J. Haah, Lattice quantum codes and exotic topological phases of matter, Ph.D. thesis, California Institute of Technology, 2013.
- [15] J. Haah, *Commun. Math. Phys.* **324**, 351 (2013).
- [16] C. Castelnovo and C. Chamon, *Philos. Mag.* **92**, 304 (2012).
- [17] C. Castelnovo, C. Chamon, and D. Sherrington, *Phys. Rev. B* **81**, 184303 (2010).
- [18] S. Bravyi and J. Haah, *Phys. Rev. Lett.* **107**, 150504 (2011).
- [19] I. H. Kim, [arXiv:1202.0052](https://arxiv.org/abs/1202.0052).
- [20] B. Yoshida, *Phys. Rev. B* **88**, 125122 (2013).
- [21] S. Bravyi and J. Haah, *Phys. Rev. Lett.* **111**, 200501 (2013).
- [22] J. Haah, *Phys. Rev. B* **89**, 075119 (2014).
- [23] I. H. Kim and J. Haah, *Phys. Rev. Lett.* **116**, 027202 (2016).
- [24] H. Ma, E. Lake, X. Chen, and M. Hermele, *Phys. Rev. B* **95**, 245126 (2017).
- [25] S. Vijay, [arXiv:1701.00762v1](https://arxiv.org/abs/1701.00762v1).
- [26] S. Vijay and L. Fu, [arXiv:1706.07070](https://arxiv.org/abs/1706.07070).
- [27] K. Slagle and Y. B. Kim, *Phys. Rev. B* **96**, 165106 (2017).
- [28] K. Slagle and Y. B. Kim, *Phys. Rev. B* **96**, 195139 (2017).
- [29] G. B. Halász, T. H. Hsieh, and L. Balents, *Phys. Rev. Lett.* **119**, 257202 (2017).
- [30] T. H. Hsieh and G. B. Halász, *Phys. Rev. B* **96**, 165105 (2017).
- [31] T. Devakul, *Phys. Rev. B* **97**, 155111 (2018).
- [32] T. Devakul, S. A. Parameswaran, and S. L. Sondhi, *Phys. Rev. B* **97**, 041110 (2018).
- [33] D. Bulmash and T. Iadecola, *Phys. Rev. B* **99**, 125132 (2019).
- [34] H. He, Y. Zheng, B. A. Bernevig, and N. Regnault, *Phys. Rev. B* **97**, 125102 (2018).
- [35] H. Ma, A. T. Schmitz, S. A. Parameswaran, M. Hermele, and R. M. Nandkishore, *Phys. Rev. B* **97**, 125101 (2018).
- [36] B. Shi and Y. M. Lu, *Phys. Rev. B* **97**, 144106 (2018).
- [37] Z. Weinstein, E. Cobanera, G. Ortiz, and Z. Nussinov, *Ann. Phys.* **412**, 168018 (2020).
- [38] Y. You, T. Devakul, F. Burnell, and S. Sondhi, *Ann. Phys.* **416**, 168140 (2020).
- [39] A. Prem, S.-J. Huang, H. Song, and M. Hermele, *Phys. Rev. X* **9**, 021010 (2019).
- [40] B. J. Brown and D. J. Williamson, *Phys. Rev. Res.* **2**, 013303 (2020).
- [41] A. T. Schmitz, S.-J. Huang, and A. Prem, *Phys. Rev. B* **99**, 205109 (2019).
- [42] Y. You, *Phys. Rev. B* **100**, 075148 (2019).
- [43] Y. You, T. Devakul, S. L. Sondhi, and F. J. Burnell, *Phys. Rev. Res.* **2**, 023249 (2020).
- [44] A. Prem and D. Williamson, *SciPost Phys.* **7**, 068 (2019).
- [45] D. Bulmash and M. Barkeshli, *Phys. Rev. B* **100**, 155146 (2019).
- [46] H. Song, A. Prem, S.-J. Huang, and M. A. Martin-Delgado, *Phys. Rev. B* **99**, 155118 (2019).
- [47] N. Tantivasadakarn, W. Ji, and S. Vijay, *Phys. Rev. B* **103**, 245136 (2021).
- [48] N. Tantivasadakarn, W. Ji, and S. Vijay, *Phys. Rev. B* **104**, 115117 (2021).

- [49] D. J. Williamson, *Phys. Rev. B* **94**, 155128 (2016).
- [50] W. Shirley, K. Slagle, and X. Chen, *SciPost Phys.* **6**, 041 (2019).
- [51] A. Kubica and B. Yoshida, [arXiv:1805.01836](https://arxiv.org/abs/1805.01836).
- [52] W. Shirley, [arXiv:2002.12026](https://arxiv.org/abs/2002.12026).
- [53] N. Tantivasadakarn, *Phys. Rev. Res.* **2**, 023353 (2020).
- [54] W. Shirley, K. Slagle, Z. Wang, and X. Chen, *Phys. Rev. X* **8**, 031051 (2018).
- [55] W. Shirley, K. Slagle, and X. Chen, *Phys. Rev. B* **99**, 115123 (2019).
- [56] T. Wang, W. Shirley, and X. Chen, *Phys. Rev. B* **100**, 085127 (2019).
- [57] W. Shirley, K. Slagle, and X. Chen, *Phys. Rev. B* **102**, 115103 (2020).
- [58] Y. You, T. Devakul, F. J. Burnell, and S. L. Sondhi, *Phys. Rev. B* **98**, 035112 (2018).
- [59] X. G. Wen, *Phys. Rev. Lett.* **90**, 016803 (2003).
- [60] G. Vidal, *Phys. Rev. Lett.* **99**, 220405 (2007).
- [61] A. Dua, P. Sarkar, D. J. Williamson, and M. Cheng, *Phys. Rev. Res.* **2**, 033021 (2020).
- [62] X. Yin, J. Zhang, and X. Wang, *Fenxi Huaxue* **32**, 1365 (2004).
- [63] T. Devakul, D. J. Williamson, and Y. You, *Phys. Rev. B* **98**, 235121 (2018).
- [64] T. Devakul, W. Shirley, and J. Wang, *Phys. Rev. Res.* **2**, 012059 (2020).
- [65] M. Levin and Z.-C. Gu, *Phys. Rev. B* **86**, 115109 (2012).
- [66] Kitaev Alexei, *Ann. Phys.* **321**, 2 (2006).
- [67] M. Levin and X.-G. Wen, *Phys. Rev. B* **67**, 245316 (2003).
- [68] See Supplemental Material at <http://link.aps.org/supplemental/10.1103/PhysRevB.107.035136> for the Mathematica file that contains the circuit V which maps the ground space of HG to that of HG .
- [69] W. Shirley, K. Slagle, and X. Chen, *Ann. Phys.* **410**, 167922 (2019).
- [70] A. Dua, I. H. Kim, M. Cheng, and D. J. Williamson, *Phys. Rev. B* **100**, 155137 (2019).
- [71] A. Dua, D. J. Williamson, J. Haah, and M. Cheng, *Phys. Rev. B* **99**, 245135 (2019).
- [72] Z. Song, A. Dua, W. Shirley, and D. J. Williamson, *PRX Quantum* **4**, 010304 (2023).
- [73] X. Ma, W. Shirley, M. Cheng, M. Levin, J. McGreevy, and X. Chen *Phys. Rev. B* **105**, 195124 (2022).
- [74] H. Song, N. Tantivasadakarn, W. Shirley, A. Vishwanath, and M. Hermele (unpublished).